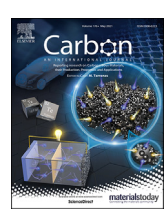


Contents lists available at ScienceDirect

Carbon

journal homepage: www.elsevier.com/locate/carbon



Research Article

Is graphite nanomesh a promising anode for the Na/K-Ions batteries?



Chen Yang ^{a, b}, Xiaotian Sun ^c, Xiuying Zhang ^a, Jingzhen Li ^a, Jiachen Ma ^a, Ying Li ^a, Linqiang Xu ^a, Shiqi Liu ^a, Jie Yang ^a, Shibo Fang ^a, Qiuhui Li ^a, Xiaoyu Yang ^{d, e, *}, Feng Pan ^f, Jing Lu ^{a, b, g, h, **}, Dapeng Yu ⁱ

- ^a State Key Laboratory for Mesoscopic Physics and Department of Physics, Peking University, Beijing, 100871, PR China
- ^b Academy for Advanced Interdisciplinary Studies, Peking University, Beijing, 100871, PR China
- ^c College of Chemistry and Chemical Engineering, And Henan Key Laboratory of Function- Oriented Porous Materials, Luoyang Normal University, Luoyang, 471934. PR China
- ^d Computer Network Information Centre, Chinese Academy of Sciences, Beijing, 100190, PR China
- ^e University of Chinese Academy of Sciences, Beijing, 100049, PR China
- f School of Advanced Materials, Peking University, Shenzhen Graduate School, Shenzhen, 518055, PR China
- ^g Collaborative Innovation Center of Quantum Matter, Beijing, 100871, PR China
- ^h Beijing Key Laboratory for Magnetoelectric Materials and Devices, Beijing, 100871, PR China
- i Shenzhen Institute for Quantum Science and Engineering and Department of Physics, Southern University of Science and Technology, Shenzhen, 518055, PR China

ARTICLE INFO

Article history: Received 6 August 2020 Received in revised form 5 December 2020 Accepted 13 December 2020 Available online 23 December 2020

Keywords:
Graphite nanomesh
Anode material
Rechargeable sodium-ion battery
Rechargeable potassium-ion battery
First-principles calculations

ABSTRACT

Nowadays, the development of promising anodes for Na and K ion batteries (NIB and KIB) has got great attention due to their sustainable and renewable energy applications. Graphite is a good candidate but suffers from low Na (<35 mAhg⁻¹) and K ion storage capacities (~274 mAhg⁻¹) in the experiments. In this paper, based on the first-principles calculations, we demonstrate that graphite nanomesh with the hole density of 46% (GN46) is a promising anode material for both the NIB and KIB. Remarkably, there are 361 —482 mAhg⁻¹ ion storage capacity for the NIB and 482—602 mAhg⁻¹ ion storage capacity for the KIB in the GN46. The in-plane diffusion barriers of Na and K ions are calculated as small as 0.59 and 0.19 eV, respectively. Besides, the holey structure opens an additional out-plane diffusing channel with only 1/14 and 1/10 of the diffusion barrier of those in graphite for Na and K ions. These diffusing properties suggest an improved rate capacity for batteries. Finally, the GN46 shows relatively small superficial area change ratio of less than 3% during the charging process, implying safety in applications. Hence, graphite nanomesh is a promising anode for the NIB and KIB.

© 2020 Elsevier Ltd. All rights reserved.

1. Introduction

Nowadays, as one of the energy supply systems, rechargeable batteries have shown wide applications ranging from personal electronics, public vehicles, and other vital areas [1–3]. To meet the increasing requirements for sustainable and renewable energy sources, the development of next-generation rechargeable batteries has never stopped. The rechargeable lithium-ion battery (LIB), which is one of the most successful energy storage systems, has

E-mail addresses: kxy@cnic.cn (X. Yang), jinglu@pku.edu.cn (J. Lu).

attracted considerable attention for years and received the 2019 Nobel prize in chemistry [4]. However, the increasing production cost and the limited lithium-element resource make LIB not the best promising future energy supply system [5]. Thus, the research of the alternative ion-battery like the sodium-ion battery (NIB) and potassium-ion battery (KIB) has sprung up due to their low cost and abundant resources of sodium/potassium elements [6,7]. Nevertheless, their further development requires finding new suitable anode materials.

Graphite is one of the most successful commercially used anodes for LIB due to its low cost, stable electrochemical performance, and the most important eligible Li-ion storage capacity of 372 mAhg⁻¹ [8]. However, the previous experimental works demonstrate that the Na-ion storage capacity is less than 35 mAhg⁻¹ [9,10], and the K ion-storage capacity is only 274 mAhg⁻¹, in

^{*} Corresponding author. Computer Network Information Centre, Chinese Academy of Sciences, Beijing, 100190, PR China.

^{**} Corresponding author. State Key Laboratory for Mesoscopic Physics and Department of Physics, Peking University, Beijing, 100871, PR China.

graphite anode [11–13]. These low storage capacities are far from the satisfaction of the applications. Silicon is another high-performance anode material for LIB with the experimental ultrahigh Li-ion storage capacity of more than 4000 mAhg⁻¹ [14]. Unfortunately, silicon is not attractive for the NIB and KIB due to both kinetical and thermodynamic limits of the Na/K-ions insertion and diffusion [15,16]. Thus, although the electrochemical properties of the NIB and KIB are similar to those of LIB, the anode materials matching well LIBs system are sometimes not suitable for the NIB and KIB, which needs further research.

Up to now, many efforts have been paid to try to improve the performance of graphite anode for the NIB and KIB, especially to understand the origin of its different Li/Na/K ion storage capacities. It is said that the different volumes of Li/Na/K ions and their various bonding with graphite make such a difference directly [13,17]. Furtherly, Goddard's group firstly got the theoretical proof that the weak adsorption energy of Na ion in graphite and the larger expanding energy for Na-ion insertion make graphite not suitable for the NIB [18]. Thus, the larger adsorption energy and the initially expanded interlayer distance are quite desirable to improve graphite anode for the NIB and KIB. Zhou's group proved that the Sdoped N-rich carbon nanosheets could expand the interlayer distance to 3.50–3.78 Å compared with that of 3.35 Å for graphite and generated 350 mAhg⁻¹ Na-ion storage capacity for the NIB in the experiment [19]. Wang's group reported a kind of expanded graphite with the interlayer distance of ~4.30 Å by a two-step oxidation-reduction process, resulting in the 284 mAhg⁻¹ Na-ion storage capacity for the NIB in the experiment [20]. Besides, Pint's group studied the N-doped graphite with the expanded interlayer distance and observed the 350 mAhg⁻¹ K-ion storage capacity for the KIB in the experiment [21]. However, the precise control of the S/N doped process and oxidation-reduction process to graphite are complex but get a very limited improvement of Na/K ions storage

In this paper, we propose a new scheme – the use of graphite nanomesh (or holey graphite) to elevate the Na/K ions storage capacities for the NIB and KIB. Such a scheme had achieved great success for the LIB in improving the Li-ion storage capacity from 372 mAhg⁻¹ to 714–1689 mAhg⁻¹ [22]. The two-dimensional (2D) similar graphene nanomesh (or holey graphene) had been successfully synthesized in many experimental works and presented the promising properties in the ion-batteries [23-27]. Herein, based on the first-principles calculations, we examine the performance of graphite nanomesh with a hole density of 46% (GN46) as the anode for the NIB and KIB. Very recently, the three-dimensional (3D) nanoporous graphite had been synthesized via a decarboxylation reaction, which possessed a very similar structure with the GN46 [28]. In our calculations, the absolute values of the adsorption energies of the single Na/K ion adsorbed in the GN46 are up to 0.39 and 1.09 eV, respectively, implying the enhanced adsorption ability of Na/K ions. After adsorption of Na/K ions, the Fermi level of the GN46 passes through the conduction band to show the enhanced electrical conductivity. The in-plane diffusion barriers of Na/K ions are as low as 0.59/0.19 eV, respectively. The holey structure opens an additional out-plane diffusing channel. These diffusion properties suggest an improved rate capacity for the NIB and KIB. Most importantly, we demonstrate that the high ion-storage capacities of $361-482 \text{ mAhg}^{-1}$ for the NIB and $482-602 \text{ mAhg}^{-1}$ for the KIB are generated in the GN46, which breaks the storage capacity limits of Na and K ions in the intrinsic graphite. Besides, the suitable average open-circle voltages of 0.26/0.54 V are also observed for the NIB and KIB in the GN46. Finally, the GN46 shows a relatively small superficial area change ratio of less than 3% during the Na/K charging process, implying safety in applications. From the above, we indicate that graphite nanomesh is a promising anode for the

NIB and KIB.

2. Computational details

The first-principles calculations were performed in the Vienna Ab initio Simulation Package (VASP) and the Cambridge Sequential Total Energy Package (CASTEP) [29–31]. The structure of the GN46 and its Na/K adsorbed compounds were firstly optimized by the VASP. And then, the energies of the GN46 and the Na/K adsorbed GN46 compounds are calculated by the 'energy' codes in the CASTEP. Our previous work has demonstrated that such a combination is precise enough [11,13,22]. Additionally, the material electronic properties, including band structures, the charge density difference, and the Bader charge analysis, were studied by the VASP due to its complete tools [32]. The climbing image nudged elastic band (CI-NEB) method was also implemented in the VASP transition state tools to calculate the diffusion pathways and barriers of Na/K ions [33,34]. The ab-initio molecular dynamics (AIMD) simulations were performed using the Nosé-Hoover thermostat at the finite temperature of 300 K with a time step of 1 fs in the VASP [35,36].

During the calculation in the VASP and CASTEP, we used the density functional theory (DFT) with a cutoff energy of 500 eV, the generalized gradient approximation (GGA) and the Perdew-Burke-Ernzerhof (PBE) form, the k-point mesh sampled by the Monkhorst–Pack method with a separation of 0.02 Å $^{-1}$, the convergence thresholds of 10^{-6} eV for energy and 10^{-3} eV/Å for force, and the plane-wave basis set with the projector-augmented wave (PAW) pseudopotential in the VASP and ultrasoft pseudopotential in the CASTEP [37,38]. Besides, we also considered the weak Van der Waals interaction by using the DFT-D3 approach in the VASP and the DFT-D correction in the CASTEP [39,40].

3. Calculation results

3.1. Structure and stability

Graphite nanomesh structures with a hole density of 35%–61% had been researched in our previous work [22]. The hole density is defined by the ratio of the area of the hexagonal hydrogen passivated holes and the unit-cell of graphite nanomesh. Our previous work showed that 46% of hole density was the best choice to generate the highest ion-storage capacity. Besides, the AA-stack graphite nanomesh model was precise enough to research the anode properties based on the previous work [22,41]. Thus, we choose the AA-stack graphite nanomesh with a hole density of 46% (GN46) to study its performance as the anodes for the NIB and KIB, which possesses the molecular formula of $C_{18}H_{6}$, as shown in Fig. 1 (a). The GN46 maintains an expanded interlayer distance of ~3.67 Å compared with that of ~3.35 Å in the intrinsic graphite. Such an expansion is due to the decreased Van der Waals' force between each holey graphene layer. Our previous work had demonstrated the thermodynamic stability of the GN46 by using the AIMD simulations [22]. To check the dynamical stability of the GN46 further, the phonon spectra are also calculated in this paper, as shown in Fig. 1 (b). Herein, the absence of an imaginary mode in the entire Brillouin zone confirms that the GN46 is dynamically stable.

3.2. Isolated Na and K atoms-adsorbed in the GN46

We first determine the favorite adsorption sites for an isolated Na/K atom adsorbed in the GN46. The typical adsorption sites with the high symmetric are considered, as shown in Fig. 2 (a), which includes the sites on the top of a carbon atom or hydrogen atom (marked as the numbers '0' ~ '2'), and the sites at the center of the

hexagonal rings (marked as the letters D/Q/R/Z). Explicitly, the 'D' and 'Z' sites are the centers of the hexagonal C—C rings; the 'Q' site is the center of the hexagonal C—H ring, and the 'R' site is the center of the hexagonal H—H ring. In each adsorption site, one isolated Na/K atom is placed, and the adsorbed structures are then optimized. The cell size of the GN46 is large enough to avoid the interaction between the Na/K atoms in different cells, based on our previous work [22]. We identify the most favorable adsorption sites of the isolated Na/K ions via calculating the adsorption energy, which is defined as:

$$E_{\rm ad} = E_{\rm MC_{18}H_6} - E_{\rm C_{18}H_6} - E_{\rm M} \tag{1}$$

where $E_{\text{MC}_{18}\text{H}_6}$, $E_{\text{C}_{18}\text{H}_6}$, and E_{M} are the total energy of the isolated Na/ K atom adsorbed GN46, the pristine GN46, and Na/K atom in the metal sodium/potassium, respectively. As shown in Fig. 2 (a), the calculated E_{ad} at the corresponding adsorption sites are summarized. For an isolated Na/K atom, the adsorption abilities in the '0' ~ '2' sites are all unstable, and the Na/K atom moves to the nearby symmetrical 'Z' sites. The favorite adsorption sites for an isolated Na/K atom are both the 'Z' site with $E_{\rm ad}$ of -0.39and -1.06 eV, respectively. Considering that the absolute values of E_{ad} for an isolated Na atom in graphite is usually about 0.2 eV (under the similar size of the unit-cell), according to the previous first-principles works, such an increase (0.19 eV) in E_{ad} of an isolated Na atom in the GN46 indicates a greatly improved Na-ion adsorption ability for the NIB [11]. [[,17] The high absolute value of E_{ad} for an isolated K atom means quite a steady adsorption, which is also about 0.26 eV higher than that (0.8 eV) of the previous calculation in graphite under the same cell, implying an improved K-ion adsorption ability for the KIB [11,13]. The 'R' sites cannot adsorb an isolated Na atom and possess feeble adsorption ability for an isolated K atom, suggesting that hydrogen atoms almost have no contribution to the Na/K atoms adsorption. As for the 'D' sites, they also possess the ability to adsorb an isolated Na/K atom, but not as strong as those of the corresponding 'Z' sites.

3.3. Electronic property of single Na and K atom-adsorbed GN46

Our previous work demonstrated that graphite nanomesh possessed the semiconductor properties when the hole density was larger than 46% [22]. For the applications as anodes, a good electrical conductivity is essential, which could be improved by the alkalis-metal atom adsorption. Thus, the electronic properties of the single Na/K ion-adsorbed GN46 (Na₁C₁₈H₆ and K₁C₁₈H₆) should

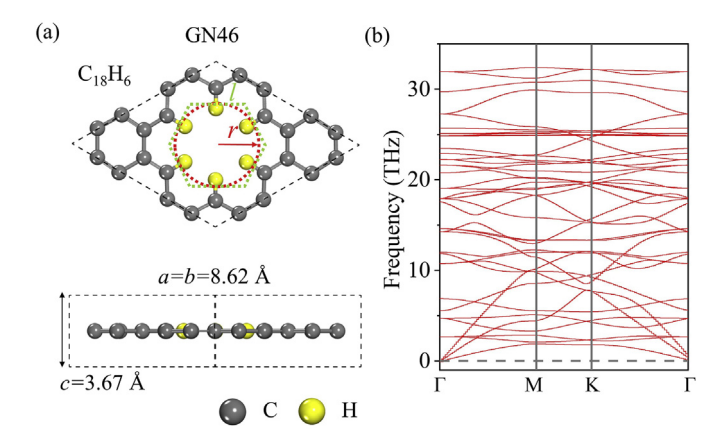


Fig. 1. (a) Optimized structures of the GN46. The blue dashed lines are the hexagonal hole, and the red dashed lines describe the tangent circle. (b) Phonon spectrum of the GN46. (A colour version of this figure can be viewed online.)

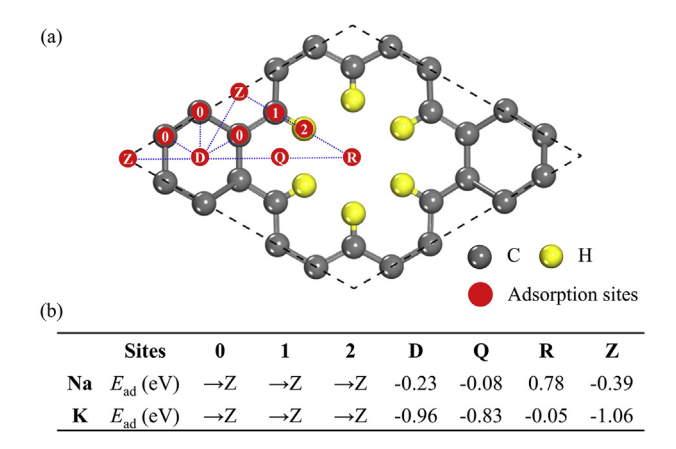


Fig. 2. (a) Symmetric adsorption sites in the GN46. (b) Adsorption energies in different adsorption sites for an isolated Na ion and K ion. (A colour version of this figure can be viewed online.)

be studied. Herein, we calculate the band structures and the corresponding total density of states (TDOS) of one Na/K atomadsorbed at the favorite 'Z' adsorption sites in the GN46 per unitcell, as shown in Fig. 3. Remarkably, after adsorbing the Na/K atoms, metallicity is generated in the GN46 due to the Fermi level across the conduction band, suggesting the enhanced electrical conductivity [42,43].

To furtherly understand the interaction between the Na/K atoms and the GN46, the charge transfers are studied in the single Na/K adsorbed GN46. Firstly, we calculate the charge density difference $(\Delta \rho)$ between the Na/K atoms and the GN46 under the definition of:

$$\Delta \rho = \rho_{\text{MGN46}} - \rho_{\text{GN46}} - \rho_{\text{M}} \tag{2}$$

where, $\rho_{\rm MGN46}$, $\rho_{\rm GN46}$, and $\rho_{\rm M}$ represent the charge density values of the Na/K adsorbed GN46, the GN46, and the single Na/K atom, respectively. As shown in Fig. 4, a net electron loss is observed above the Na/K atoms, and a net electron gain occurs between Na/K atoms and the nearby carbon atoms. Electron transfers happen from the Na/K atoms to the GN46, indicating an ionic interaction between the Na/K atoms and the GN46. To further calculate the specific amount of electron transfers, we perform Bader charge analysis and find that Na/K atoms act as the electron donors and donate about $0.81/0.85~e^-$ per atom to the GN46, respectively. These results indicate that Na/K atoms are the ionic state after adsorbed in the GN46, which caters to the application as anodes for the ion batteries.

3.4. Diffusion barriers of single Na and K ions

To evaluate the rate capacity of the materials used as an anode for the ion batteries, the diffusion barrier of the single ion in the anode is an essential reference. [44,45] Herein, due to the 3D holey structure of the GN46, there are two kinds of diffusion directions for Na/K ions, including the horizontal in-plane pathway and the vertical out-plane pathway. For comparison, we also calculate the diffusion barriers of Na/K ion diffusing in the intrinsic graphite under the same unit-cell with the GN46.

For the in-plane diffusion direction, the diffusion pathways of Na/K ions diffusing in graphite and the GN46 are marked, as shown in Fig. 5 (a). Based on the previous work, the Na/K ions started from the center of the C—C ring and diffused to the symmetrical adjacent center site in graphite [46]. However, due to the holey structure in the GN46, there are two possible diffusion pathways named A and B pathways, respectively. In the A-pathway, the Na/K ions diffuse only

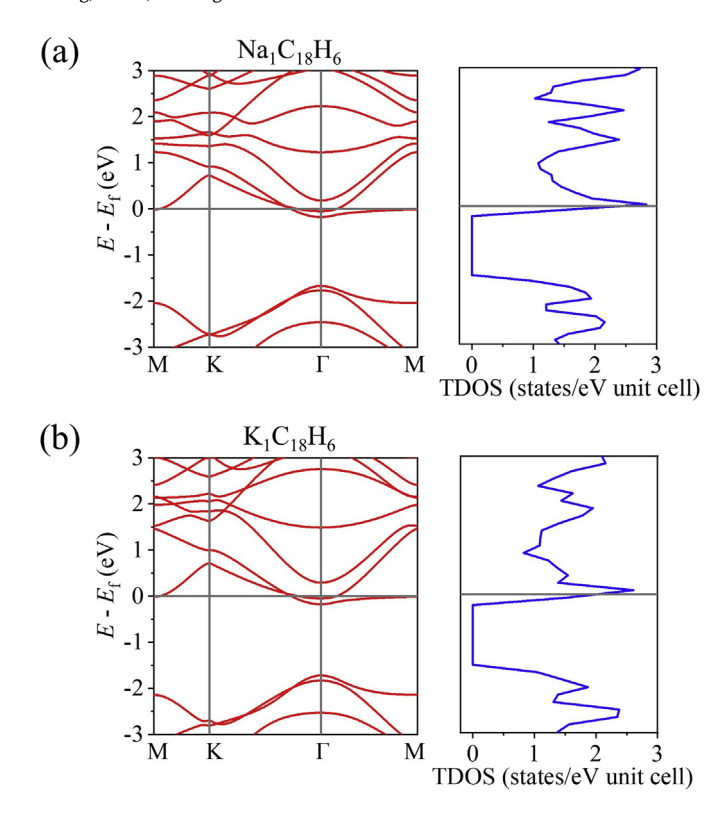


Fig. 3. Band structure and total density of states (TDOS) of one (a) Na ion and (b) K ion adsorbed in the GN46. The Fermi level is set to zero. (A colour version of this figure can be viewed online.)

at the surface of the residual graphite along 'Z' \rightarrow 'D' \rightarrow 'Z' sites. In the B-pathway, the Na/K ions bypass the edge of the hydrogen passivated hole along 'Z' \rightarrow 'Q' \rightarrow 'Z' sites. As shown in Fig. 5 (b), the diffusion barriers are about 0.48 and 0.19 eV for the single Na and K ions in graphite, respectively. As for the GN46, the diffusion barriers of Na/K ions are about 0.59 and 0.19 eV for A-pathway, and 0.61 and 0.22 eV for B-pathway. Thus, Na/K ions prefer diffusing through the A-pathway with lower diffusion barriers of 0.59 and 0.19 eV, respectively. Remarkably, the diffusion barrier of single Na ion in the GN46 is a little higher than that in graphite. Such an increased diffusion barrier of Na ion in the GN46 might be contributed to the quite improved adsorption ability in the GN46 compared with the feeble adsorption ability of Na ion in graphite [46—48]. The

adsorption of Na ion makes more interaction between the Na ion and the GN46, leading to a higher diffusion barrier. Similarly, the diffusion barrier of the single K ion in the GN46 demonstrates almost no difference with that in graphite due to both the adsorption ability of K ion in the GN46 and graphite.

The additional vertical out-plane diffusion channels are crucial for the accelerated charging/discharging process, as reported in the previous studies [44,45]. As shown in Fig. 6 (a), for graphite, the diffusion barriers for Na/K ions diffusing across the hollow site in a C–C hexagon are calculated as large as 21.43 and 25.60 eV, respectively, indicating an nearly impossible diffusing process and the absence of the ability of vertical out-plane diffusion. By contrast, as shown in Fig. 6 (b), the calculated diffusion barriers for the Na/K ions travel through the hydrogen passivated hole in the GN46 are about 1.51 and 2.62 eV, respectively, which are only about 1/14 and 1/10 of those in graphite, implying an accelerated charging/discharging process for the NIB and KIB. Both the low inplane diffusion barriers and the additional out-plane diffusion channels guarantee a good rate capacity of the GN46 for the NIB and KIB.

3.5. Maximum Na and K ions-storage capacity

As discussed before, the initial expanded interlayer distance and the larger adsorption energy are both naturally satisfied in the GN46, which are essential for elevating the ion storage capacities for the NIB and KIB in graphite [18]. In this part, we research whether the maximum Na/K ion storage capacities are indeed improved in the GN46.

The Na/K ion storage capacity is calculated from the equation:

$$C = \frac{1}{W_{Anode}} \times x \times F \tag{3}$$

where W_{Anode} is the atomic Molar weight of the GN46 or graphite anodes per unit-cell, x is the number of the adsorbed Na/K ions in the GN46 or graphite anodes, and F is the Faraday constant.

Besides, the average adsorption energy (E_{ave}) per Na/K atoms could be defined as:

$$E_{\text{ave}} = \frac{E_{\text{M}_x \text{C}_{18} \text{H}_6} - E_{\text{C}_{18} \text{H}_6} - x E_{\text{M}}}{x} \tag{4}$$

where $E_{M_xC_{18}H_6}$, $E_{C_{18}H_6}$, and E_M are the total energy of the Na/K adsorbed GN46, the pristine GN46, and per Na/K atom in the metal sodium/potassium, respectively. Besides, x is the number of Na/K

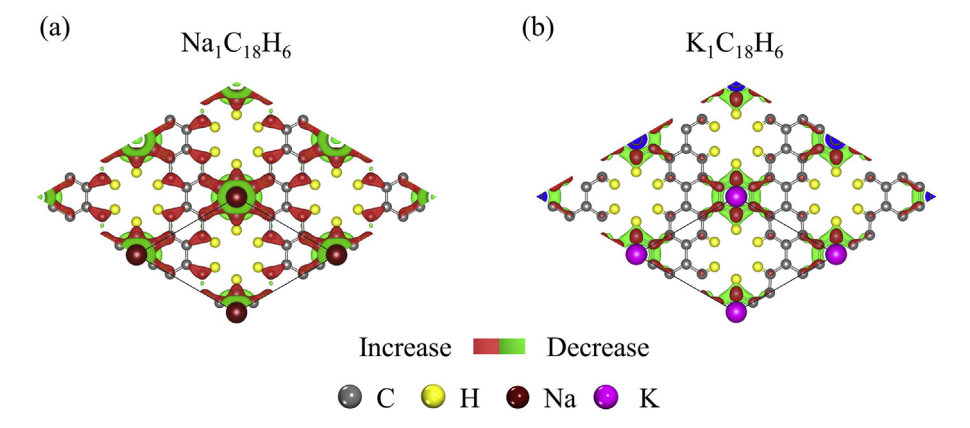


Fig. 4. Top views of charge density difference for one (a) Na ion and (b) K ion adsorbed in the GN46. Red and green colors indicate the net increase and decrease of electrons. (A colour version of this figure can be viewed online.)

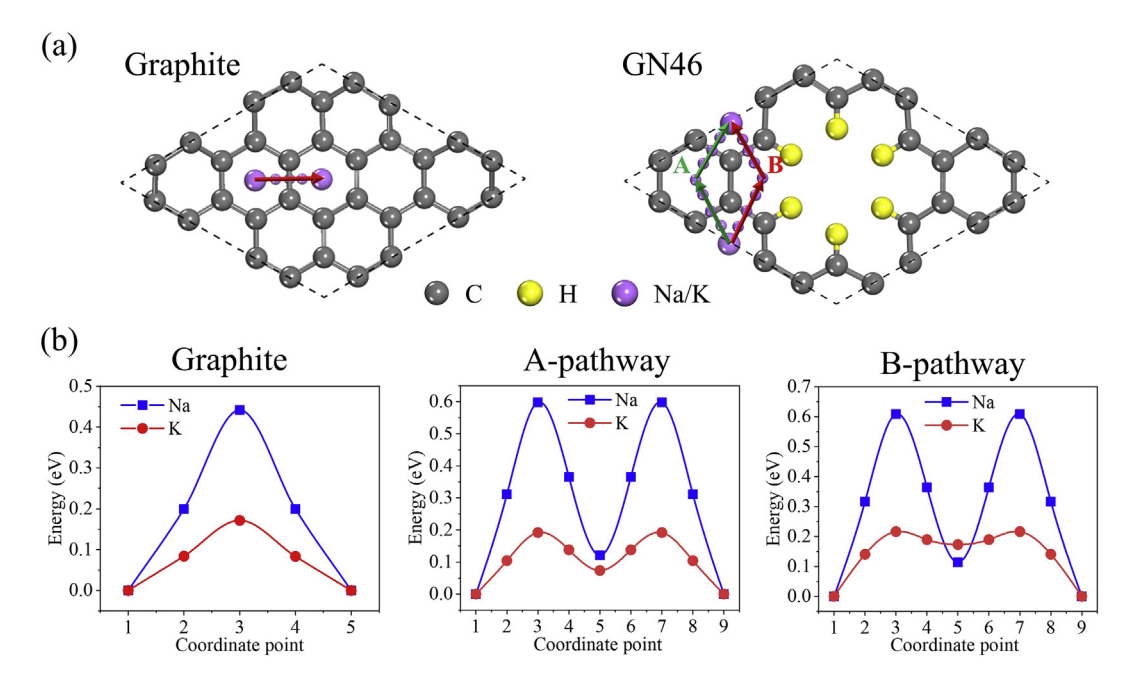


Fig. 5. (a) In-plane diffusion pathways of one Na and K ion diffusing at the interlayer of the graphite and the GN46. (b) The corresponding in-plane diffusion energy profiles. (A colour version of this figure can be viewed online.)

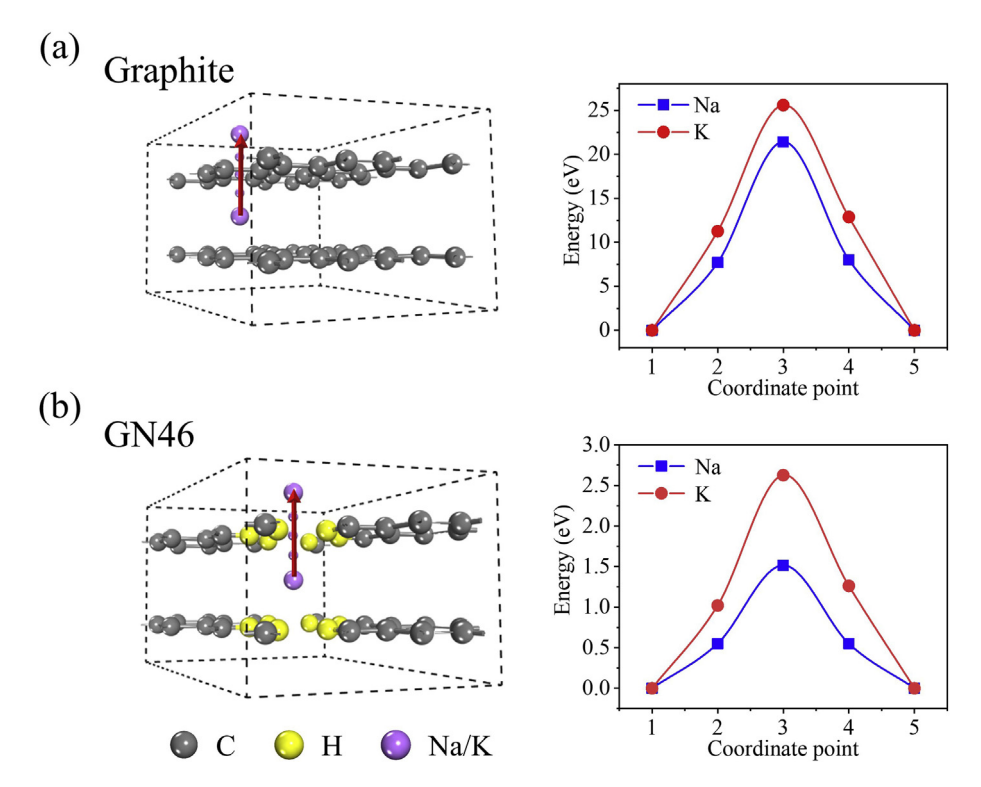


Fig. 6. Out-plane diffusion pathways and diffusion energy profile of one Na and K ion through the hole of (a) the graphite and (b) the GN46. (A colour version of this figure can be viewed online.)

atoms adsorbed in the GN46. As the thermodynamical criterion, to make the adsorption process for the Na/K atoms could occur spontaneously, $E_{\rm ave}$ should be negative. A larger absolute value of $E_{\rm ave}$ indicates a higher adsorption ability with a more stable

isolated Na/K atom adsorbed structure.

In many previous theoretical works, the energetically critical point where the sign of E_{ave} is changed from a negative (energetically favorable) to a positive value (energetically unfavorable) is

usually regarded as the criterion to determine the maximum x and thus the maximum ion storage capacities for the anode materials [22,35,36,44,49]. However, such a thermodynamical criterion does not work for Li-ion storage in graphite anode. On the experimental aspect, graphite anode could only generate less than 35 mAhg⁻¹ Na-ion storage capacity [17,18,20]. But on the theoretical aspect, the critical point of $E_{\rm ave}$ has a stoichiometry NaC₁₂, corresponding to a maximum Na-ion storage capacaity of ~186 mAhg⁻¹ [11,13,18]. As for the K ions, the previous experimental studies demonstrated that the KC₈ structure is the adsorption limit in graphite, but the calculated $E_{\rm ave}$ at this concentration is about -0.4 eV [12]. The structure of KC₆ also possesses $E_{\rm ave}$ of about -0.2 eV in the theoretical studies, but it is not observed experimentally [11,13].

There are two possible causes for such a discrepancy: (1) The actual insertion of metal ions into graphite not only depends on the total energy difference of the reactant and product but also depends on the kinetics, especially when the system is under low adsorption energy, which often implies a high reaction barrier [11–13,15,16]. (2) The effect of entropy is not considered at all in these theoretical calculations.

As shown in Fig. 7., our calculated adsorption energies per Na/K ion in graphite are about 0.08 eV (NaC₁₂), 0.05 eV (NaC₈), -0.39 eV (KC₁₂), -0.43 eV (KC₈) and -0.23 eV (KC₆), which are consistent with the previous work (NaC₁₂: 0.03 eV, NaC₈: 0.05 eV, KC₁₂: -0.38 eV, KC₈: -0.42 eV, and KC₆: -0.22 eV) [11,13]. The reported values of $E_{\rm ave}$ are negative before NaC₁₂ but their absolute values are all smaller than 0.2 eV in Na-adsorbed graphite. The reasonable threshold value of $E_{\rm ave}$ should be corrected to -0.2 and -0.4 eV, respectively, to reproduce the observed Na and K ion storage capacity in intrinsic graphite. Thus we set $E_{\rm ave} = -0.2$ and -0.4 eV as the more realistic criterion (or kinetic criterion) for obtaining the maximum x and storage capacity in graphite-like materials (GN46) for Na and K ions, respectively.

For the GN46, at the low Na/K ions storage capacities, $E_{\rm ave}$ keeps negative and indicates that the Na/K ions can be adsorbed in the GN46 quite steadily instead of clustering to form Na/K metals. With the increase of the ion concentration, the electrostatic attractions between the GN46 hosts and the Na/K ions become weaker, and the Na–Na or K–K ions interactions are enhanced [22,35,43,49,50]. Thus, the absolute values of $E_{\rm ave}$ for both Na/K ions are becoming smaller. However, these values are still larger than those of graphite under the same Na/K ion storage capacities, implying that the holy structure has stabilized Na/K ion. As a result, the Na-ion storage capacity is ~482 mAhg⁻¹ (Na₄C₁₈H₆) under the thermodynamical criterion and ~361 mAhg⁻¹ (Na₃C₁₈H₆) under the more realistic criterion. Similarly, the GN46 possesses the K-ion storage capacity

of ~602 mAhg $^{-1}$ (K₅C₁₈H₆) under the thermodynamical criterion and ~482 mAhg $^{-1}$ (K₄C₁₈H₆) under the more realistic criterion for the KIB. Considering that graphite possesses low experimental Naion storage (<35 mAhg $^{-1}$) and K-ion storage (~274 mAhg $^{-1}$) capacities, these values of Na-ion and K-ion storage capacities in the GN46 are quite a significant improvement [17,18].

Finally, we perform the AIMD to check the thermodynamic stability of the maximum Na/K ions adsorbed structures at room temperature, as shown in Fig. S1. As a result, the total energies of Na₃C₁₈H₆, Na₄C₁₈H₆, K₄C₁₈H₆, and K₅C₁₈H₆ are all kept stable during the AIMD simulations of up to 5000 fs. Besides, the structures of those compounds are all kept steady with feeble deformation after 5000 fs. These results suggest that the maximum Na/K ions adsorbed structures are thermodynamically stable at room temperature [35,36].

3.6. Open-circuit voltage for the NIB and KIB

When the GN46 is used as anodes for the NIB and KIB, the charging/discharging process can be summarized as:

$$(x_2 - x_1)M^+ + (x_2 - x_1)e^- + M_{x_1}C_{18}H_6 \leftrightarrow M_{x_2}C_{18}H_6$$
 (5)

Thus, when the pressure, volume, and entropy effects are neglected, the open-circuit voltage (OCV) of the GN46 can be calculated as:

$$V \approx \frac{E_{M_{x_1}C_{18}H_6} - E_{M_{x_2}C_{18}H_6} + (x_2 - x_1)E_M}{(x_2 - x_1)e}$$
 (6)

where $E_{M_{x_1}C_{18}H_6}$, $E_{M_{x_2}C_{18}H_6}$ and E_{M} are the total energy of $M_{x_1}C_{18}H_6$, $M_{x_2}C_{18}H_6$, and per Na/K atom in the metal sodium/potassium, respectively.

As shown in Fig. 8, in the open-circuit voltage profiles, commonly, there are three prominent regions: (1) plateau region with weak Na–Na or K–K interactions at the low ion concentration, (2) the increase of repulsive interaction between the Na–Na or K–K ions, (3) strong repulsive interaction with a negative voltage [51,52]. The first and second regions stand for the reversible regions used as an anode, which are marked green and orange colors. However, the gray regions demonstrate the irreversible parts due to the negative values of voltages [22,51,52]. Remarkably, the GN46 could generate the reversible Na-ion storage capacity of 361 mAhg $^{-1}$ (Na₃C₁₈H₆) and K-ion storage capacity of 482 mAhg $^{-1}$ (K₄C₁₈H₆). The reversible Na and K-ion storage capacity values are about 75% and 80% of those of the corresponding maximum Na and

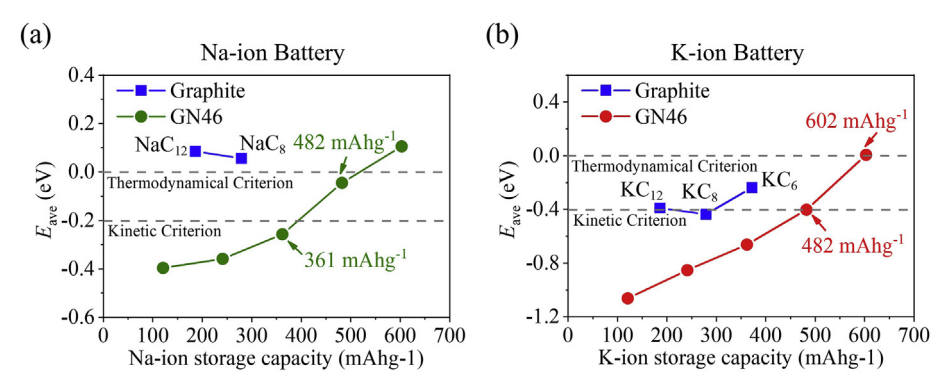


Fig. 7. Average adsorption energy (E_{ave}) versus the ion-storage capacity in the GN46 for (a) Na-ion battery and (b) K-ion battery. The average adsorption energies of Na ion and K ion adsorbed in the graphite are also calculated for comparison. Gray dashed lines stand for the kinetic and thermodynamical criteria to determine the maximum storage capacity. (A colour version of this figure can be viewed online.)

K ions storage values in the GN46. We should state that those irreversible storage capacities are due to the half-cell reaction because we only research the anode part of the battery. The previous works showed that when the anode is connected to a full-cell, the external voltage could overcome the irreversible storage capacity and charge the anode to the theoretical maximum ion storage capacity [22,51,52].

Before being charged with the maximum ion storage capacities, the OCV for the NIB decreases from 0.39 V to 0.06 V with an average value of 0.26 V. Similarily, the average OCV for the KIB is 0.54 V. Generally, a low average OCV of materials, when used as the anode, guarantees a high energy density and a high output voltage. The previous studies show that the suitable average OCV should be in the range of 0.2–1 V for the anodes [53]. Fortunately, the average OCVs of the GN46 are suitable for both the NIB and KIB, which makes the GN46 suitable candidates to be used as the anode.

3.7. Safety in applications

From the discussion above, we can get the preliminary judgment that the GN46 is a promising anode material with the high-performance properties like the low diffusion barriers for Na/K ions and the high Na/K ion storage capacities. However, for the experimental application, the safety of the anode is quite important.

For instance, during the charging process, there is usually some structure expansion in the anode, which is also sensitive to the material cycle stability [14,50]. The significant surface area expansion of the anodes might cause electrode pulverization and eventually lead to fast capacity fading and even potential safety hazards. Thus, we test the surface area expansion of the Na/K ions adsorbed GN46 firstly. Following the previous study, the superficial areachange ratio (ΔS) could be defined as [22,50].

$$\Delta S = \left[\left(S_{\text{M},\text{GN46}} - S_{\text{GN46}} \right) / S_{\text{GN46}} \right] \times 100\% \tag{7}$$

where $S_{\rm M_x GN46}$ and $S_{\rm GN46}$ are the superficial area per unit-cell of the Na/K ion adsorbed anodes and the intrinsic anodes, respectively [22,50].

We calculate the superficial area-change ratio of graphite and the GN46 as a function of Na/K ion storage capacities, as shown in Fig. 9. With the increase of the ion storage capacities, the superficial area-change ratios of both graphite and the GN46 are getting larger due to the more and more ions inserting. Remarkably, at each of the same Na/K ion storage capacities, the superficial area-change ratio of graphite is higher than those of the GN46. Finally, when the

GN46 get their maximum Na/K ion storage capacities, the superficial area-change ratios are both less than 3% for the NIB and KIB, implying very little expansion in applications, which is essential to the safety in applications.

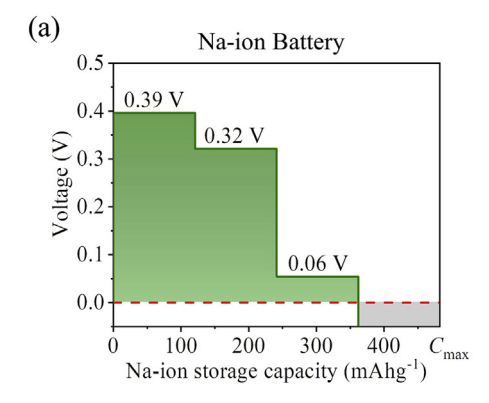
Besides, when the anode materials are adsorbed with a high concentration of ions, the ions would sometimes get together to generate the clusters and lead to the dendrites. These dendrites would break the anode structure, leading to a potential safety hazard. Herein, under the maximum Na/K ion storage capacities, we check whether the Na/K ions are still ionic state by calculating the electron localization functions (ELFs) and the charge density difference ($\Delta \rho$) for the Na₄C₁₈H₆ and K₅C₁₈H₆, as shown in Fig. 10 and Fig. S2, respectively. As a result, the electrons are almost localized in the Na/K ions and the GN46 substrate. The regions between the Na/K ions and the GN46 always show the ELF ~0, and a net electron gain occurs between Na/K ions and the nearby holey graphene layer. Additionally, the regions between each Na or K ions are also ELF ~0, and a net electron loss is observed around the Na/K ions. These results suggest that Na/K ions still keep ionic state even under the maximum Na/K ions adsorption instead of clustering to form Na/K metals, which is essential to prevent the generation of the dendrites when used as anodes for the NIB and KIB [49].

Finally, the charge transfers per ion as a function of the metal/C ratio are also calculated to demonstrate the electrochemical stability of the GN46. Herein, those of graphite is also calculated for comparison. As shown in Fig. 11, the charge transfers are kept about $0.8 e^{-}$ per ion from Na ions to the GN46 when it used as the anode for the NIB. As for the KIB, the charge transfers show a small decrease with the increase of the metal/C ratio but are still all larger than $0.7 e^-$ per ion from K ions to the GN46. For the Na ions, the charge transfers are almost equal for graphite and the GN46. However, as for the K ions, the charge transfers demonstrate the increase in the GN46, compared with those in graphite as the same K/C ratio. These results indicate that the strong ion bonds are always formed between the GN46 and the Na/K ions, and such bonding is even enhanced in the GN46 for K ions compared with graphite, indicating that the electrochemical processes are stable when the GN46 is used as anodes for the NIB and KIB [50].

4. Discussion

4.1. Comparing Na/K ion storage capacities with other carbon-based materials

Carbon-based material usually possesses low production prices for its readily available from nature, which is a kind of desirable



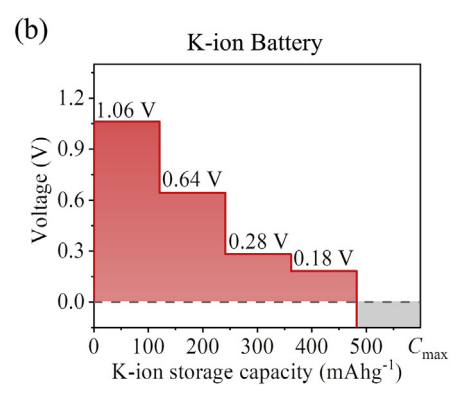


Fig. 8. Open-circle voltage (OCV) profiles as a function of ion storage capacity in the GN46 for the (a) Na-ion battery and (b) K-ion battery. The green and orange regions stand for the reversible parts, and the gray regions demonstrate the irreversible parts, respectively. (A colour version of this figure can be viewed online.)

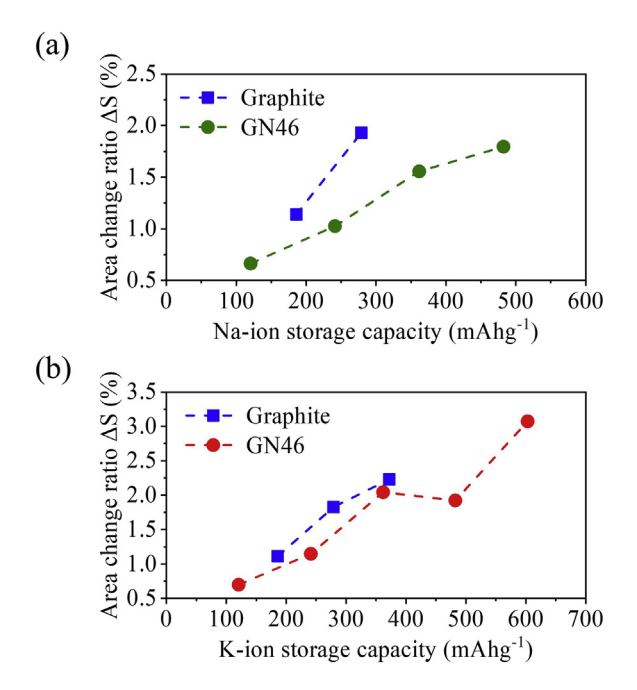
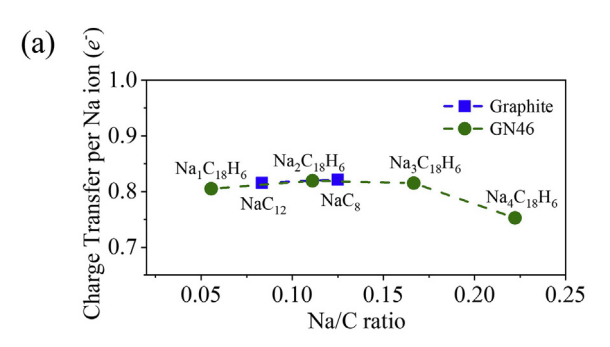


Fig. 9. Superficial area-change ratio as a function of (a) the Na-ion storage capacity and (b) the K-ion storage capacity. Those of the graphite are also listed for comparison. (A colour version of this figure can be viewed online.)

sustainable energy material. Many works have been demonstrated for the potential application of carbon-based materials as the anode for the NIB and KIB. Herein, we compare the Na/K ion storage capacities of the GN46 with other representative carbon-based materials when used as anodes for the NIB and KIB, as shown in Table 1 and Table 2, respectively. Obviously, graphite shows quite low storage capacities for Na and K ions. Besides, it shows that the sample preparations of the other carbon-based materials are sometimes complex. However, the improvement of Na/K ion storage capacity is still limited in those carbon-based materials. As for GN46, our calculated results demonstrate the high ion-storage capacity of 361–482 mAhg⁻¹ for the NIB and 361–482 mAhg⁻¹ for



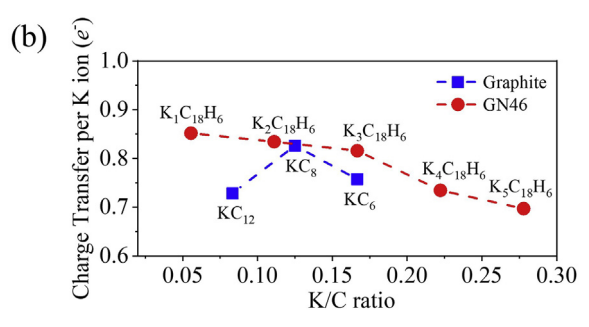


Fig. 11. Charge transfer per metal ion as a function of metal/C ratio for (a) Na and (b) K. Those of the graphite are also listed for comparison.

the KIB, which is among the best of candidates for carbon-based materials. Besides, it is not surprising to find that the non-graphitizing carbons (hard carbons), which are partially close to the GN46 in the holey structures, commonly possess relatively high ion-storage capacities in the experiments.

4.2. The origin of the improved Na/K ion-storage capacities in the GN46

We should state that the improved theoretical maximum Na/K ion storage capacity in the GN46 does not owe to the Na/K ions adsorbed in the hole space, which could be reflected from the conclusion that the hydrogen atoms almost have no contribution to

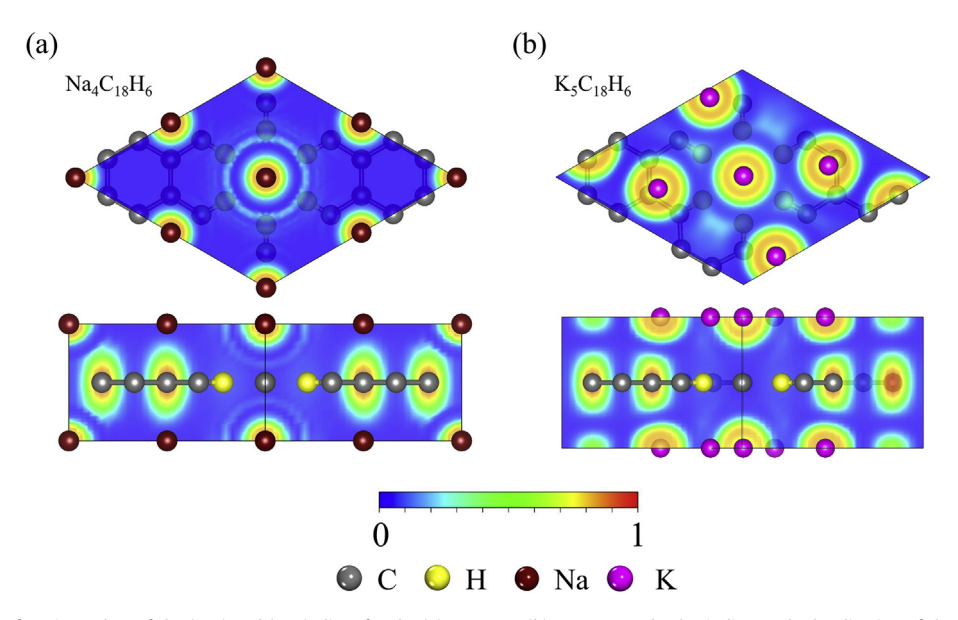


Fig. 10. Electron localization functions plots of the (110) and (001) slices for the (a) $Na_4C_{18}H_6$ (b) $K_5C_{18}H_6$. Red color indicates the localization of the valence electrons, and blue means no valence electron here. (A colour version of this figure can be viewed online.)

Table 1Summary of the sample preparation and Na-ion storage capacity for representative carbon-based materials when used as anodes for the NIB.

Carbon-based Materials	Sample Preparation	Capacities $(mAhg^{-1})$	Ref.
N/P co-doped carbon microspheres	Hydrothermal process	545	[54]
O-doped 3D carbonaceous	Epitaxial growth method	430	[55]
Graphite nanomesh		361~482	This work
Hard carbon	One method for manufacturing activated carbon [56]	386	[57]
	Carbonized at 1350 °C for 2 h	336.4	[58]
	Carbonized at 1500 °C for 2 h	330	[59]
	Carbonized at 1000-1600 °C	319	[60]
S-doped N-rich carbon nanosheets	S/N doped process	350	[19]
P-doped hard carbon	P-doped process	328	[61]
3D porous carbon frameworks	Mixing acetone and NaOH	303.2	[62]
N-Doped graphene foams	Annealing the freeze-dried graphene oxide foams	291	[63]
Expanded graphite oxide	Two-step oxidation-reduction process	284	[20]
Porous carbon/graphene composite	Facile ionothermal process	250	[64]
Disordered 3D multi-layer graphene	CO ₂ gas through a reaction with Li	190	[65]
Graphite	_	<35	[8]

Table 2Summary of the sample preparation and K-ion storage capacity for representative carbon-based materials when used as anodes for the KIB.

Carbon-based Materials	Sample Preparation	Capacities (mAhg ⁻¹)	Ref.
Graphite nanomesh	_	482-603	This work
Hard carbon porous nanobelts	Carbonized at 650 °C under argon atmosphere	468	[66]
Polynanocrystalline graphite	Chemical vapor deposition	387	[67]
N-doped graphite	N-doped process	350	[21]
S/N co-doping graphene nanosheets	S/N co-doped process	348.2	[68]
Hard carbon	One method for manufacturing activated carbon [56]	336	[57]
	Carbonizing the renewable piths of sorghum stalks	304.6	[69]
P-doped hard carbon	P-doped process	302	[61]
Graphite	_	274	[8]
Highly N-doped carbon nanofibers	Polypyrrole carbonized in N ₂	248	[70]

the Na/K ions adsorption. Considering the ion storage capacity could be calculated by the equation of $C = \frac{1}{W_{anode}} \times x \times F$, the following three reasons might contribute to the higher Na/K ion storage capacities: (1) A larger interface distance of 3.67 Å was generated in the GN46, in comparison with that of 3.35 Å for graphite, which could produce a wider space for ion storage capacity per unit-cell, leading to a bigger x_{max} . (2) The increased adsorption energies of Na/K ions in the GN46 compared with those in graphite under the same ion concentrations contribute to more ions adsorption, benefiting a bigger x_{max} . (3) A lower atomic Molar weight of the GN46 per unit-cell with a value of 77% of that of graphite under the same unit-cell size, suggesting a smaller W_{anode} .

4.3. Creating graphite nanomesh samples in the future

Although the GN46 is a priming anode material for the NIB and KIB, we have to claim that it is still a kind of prophetic material. However, many previous works demonstrate the possibility of the fabrication of such a graphite nanomesh. For instance, in 2018, the nanoporous graphene (NPG) has been bottom-up synthesized by Mugarza's group [23,24]. The hole size in the NPG is less than 1 nm, and the holey structure in the NPG is very similar to that in the GN46. Besides, Duan's group has successfully created graphene nanomesh (GN) by using top-down approaches of O₂ plasma exposure in 2019 [25,26]. The hole size in the GN is also smaller than 1 nm. Furthermore, Yang's group had successfully experimentally obtained small-sized nanoporous graphene via a hierarchical reaction pathway on Au(111), which is indeed the 2D structure of the similar graphite nanomesh [27]. Finally, the threedimensional (3D) similar nanoporous graphite had also been synthesized via a decarboxylation reaction [28]. These experimental methods provide the possibility of creating graphite nanomesh

anode, which deserves more effort in the future.

4.4. Diffusion of organic solvent molecules

In the actual case, the organic solvent such as carbonate is often used as the electrolyte solvent. There is a concern that these molecules could probably diffuse to the matrix to be electrochemically decomposed in the porous anode materials. However, the pore size in the GN46 is ~0.37 nm, which is equal to, or smaller than, the sizes of many kinds of the electrolyte ions like ethylene carbonate (EC, ~0.40 nm) [71], propylene carbonate (PC, ~0.39 nm) [72], and ethyl methyl carbonate (EMC, ~0.90 nm) [73]. Thus, it is commonly hard for these electrolyte ions to diffuse into the matrix through the pore. Besides, even if several electrolyte ions could probably diffuse into the GN46, the narrow interlayer spacing of the GN46 (<1 nm) could probably weaken the interactions of organic solvents by space restriction and tend to generate the more ordered structures of the metal ions-organic solvents composites, as reported in Q. Cai's study [73]. Thus, the decomposition of electrolyte ions would probably be restrained in the GN46. Finally, there would usually generate a layer of solid electrolyte interphase (SEI) at the surface for the carbon-based anodes, preventing the diffusion of organic solvent [74]. From these previous references, we tentatively conclude that the GN46 is still a promising anode material in the experiment when faced with the organic solvent.

5. Conclusion

In this paper, the first-principles calculations were performed to examine the properties of graphite nanomesh with the hole density of 46% (GN46) used as anodes for the NIB and KIB. We found that the GN46 was a promising anode material for the NIB and KIB with the following good characters: (1) a larger absolute value of $E_{\rm ad}$ for

the isolated Na/K ions (indicating a higher adsorption ability with the more stable Na/K adsorbed structure), (2) an enhanced electrical conductivity (benefit to the application as anodes for ion batteries), (3) a low in-plane diffusion barriers of 0.59/0.19 eV for single Na/K ion and the additional out-plane diffusing channel through the holey structure (suggesting good cycle stability for the NIB and KIB), (4) high ion-storage capacities of 361–482 mAhg⁻¹ for the NIB and 361–482 mAhg⁻¹ for the KIB (breaking the storage capacity limits of Na and K ions in graphite), (5) suitable average OCV of 0.26/0.54 V for the NIB and KIB, (6) relatively small structure deformations during the Na/K charging process and the stable electrochemical process (implying safety in use).

CRediT authorship contribution statement

Chen Yang: is the first author of this paper. He finished all the calculations and this manuscript. Xiaotian Sun: are co-authors who participate in the discussions. Xiuying Zhang: are coauthors who participate in the discussions. Jingzhen Li: are coauthors who participate in the discussions. Jiachen Ma: are coauthors who participate in the discussions. Ying Li: are coauthors who participate in the discussions. Linqiang Xu: are coauthors who participate in the discussions. Shiqi Liu: are coauthors who participate in the discussions. Jie Yang: are coauthors who participate in the discussions. Shibo Fang: are coauthors who participate in the discussions. Qiuhui Li: are coauthors who participate in the discussions. Xiaoyu Yang: are the co-corresponding authors who provide the guidance of this work. **Feng Pan:** are the group leaders who also give the support to this work. Jing Lu: are the co-corresponding authors who provide the guidance of this work. Dapeng Yu: are the group leaders who also give the support to this work.

Declaration of competing interest

The authors declare that they have no known competing financial interests or personal relationships that could have appeared to influence the work reported in this paper.

Acknowledgment

This work was supported by the Ministry of Science and Technology of China (No. 2016YFB0700600 (National Materials Genome Project) and 2017YFA206303), the National Natural Science Foundation of China (No. 11674005, 91964101, and 11664026), the Highperformance Computing Platform of Peking University and the MatCloud + high throughput materials simulation engine.

Appendix A. Supplementary data

Supplementary data to this article can be found online at https://doi.org/10.1016/j.carbon.2020.12.039.

References

- [1] J. Tarascon, M. Armand, Issues and challenges facing rechargeable lithium batteries, Nature 414 (6861) (2001) 359–367.
- [2] P. Bruce, B. Scrosati, J. Tarascon, Nanomaterials for rechargeable lithium batteries, Angew. Chem. Int. Ed. 47 (16) (2008) 2930–2946.
- [3] J. Goodenough, Y. Kim, Challenges for rechargeable Li batteries, Chem. Mater. 22 (3) (2010) 587–603.
- [4] P. Kamat, Lithium-ion batteries and beyond: celebrating the 2019 Nobel prize in chemistry — a virtual issue, ACS Energy Lett. 4 (11) (2019) 2757—2759.
- [5] J. Tarascon, Is lithium the new gold? Nat. Chem. 2 (6) (2010), 510-510.
- [6] D. Bin, X. Lin, Y. Sun, Y. Xu, K. Zhang, A. Cao, L. Wan, Engineering hollow carbon architecture for high-performance K-ion battery anode, J. Am. Chem. Soc. 140 (23) (2018) 7127–7134.
- [7] N. Yabuuchi, K. Kubota, M. Dahbi, S. Komaba, Research development on

- sodium-ion batteries, Chem. Rev. 114 (23) (2014) 11636-11682.
- [8] Y. Li, Y. Lu, P. Adelhelm, M. Titirici, Y. Hu, Intercalation chemistry of graphite: alkali metal ions and beyond, Chem. Soc. Rev. 48 (17) (2019) 4655–4687.
- [9] P. Ge, M. Fouletier, Electrochemical interaction of sodium in graphite, Solid State Ionics 28–30 (1988) 1172–1175.
- [10] D. Stevens, J. Dahn, The mechanisms of lithium and sodium insertion in carbon materials, J. Electrochem. Soc. 148 (2001) A803—A811.
- [11] W. Wan, H. Wang, Study on the first-principles calculations of graphite intercalated by alkali metal (Li, Na, K), Int. J. Electrochem. Sc. 10 (4) (2015) 3177–3184.
- [12] Z. Jian, W. Luo, X. Ji, Carbon electrodes for K-ion batteries, J. Am. Chem. Soc. 137 (36) (2015) 11566–11569.
- [13] K. Nobuhara, H. Nakayama, M. Nose, S. Nakanishi, H. Iba, First-principles study of alkali metal-graphite intercalation compounds, J. Power Sources 243 (2013) 585–587.
- [14] C. Chan, H. Peng, G. Liu, K. Mcilwrath, X. Zhang, R. Huggins, Y. Cui, High-performance lithium battery anodes using silicon nanowires, Nat. Nanotechnol. 3 (1) (2008) 31–35.
- [15] S. Komaba, Y. Matsuura, T. Ishikawa, N. Yabuuchi, W. Murata, S. Kuze, Redox reaction of Sn-polyacrylate electrodes in aprotic Na cell, Electrochem. Commun. 21 (2012) 65–68.
- [16] V. Chevrier, G. Ceder, Challenges for Na-ion negative electrodes, J. Electrochem. Soc. 158 (2011) A1011—A1014.
- [17] H. Moriwake, A. Kuwabara, C. Fisher, Y. Ikuhara, Why is sodium-intercalated graphite unstable? RSC Adv. 7 (58) (2017) 36550–36554.
- [18] Y. Liu, B.V. Merinov, W. Goddard, Origin of low sodium capacity in graphite and generally weak substrate binding of Na and Mg among alkali and alkaline earth metals, P. Natl. Acad. Sci. USA. 113 (14) (2016) 3735–3739.
- [19] J. Yang, X. Zhou, D. Wu, X. Zhao, Z. Zhou, S-Doped N-rich carbon nanosheets with expanded interlayer distance as anode materials for sodium-ion batteries, Adv. Mater. 29 (6) (2017) 1604108.
- [20] Y. Wen, K. He, Y. Zhu, F. Han, Y. Xu, I. Matsuda, Y. Ishii, J. Cumings, C. Wang, Expanded graphite as superior anode for sodium-ion batteries, Nat. Commun. 5 (1) (2014) 4033.
- [21] K. Share, A. Cohn, R. Carter, B. Rogers, C. Pint, Role of nitrogen doped graphene for improved high capacity potassium-ion battery anodes, ACS Nano 10 (2016) 9738–9744.
- [22] C. Yang, et al., Holey graphite: a promising anode material with ultrahigh storage for lithium-ion battery, Electrochim. Acta 346 (2020) 136244.
- [23] C. Moreno, et al., Bottom-up Synthesis of multifunctional nanoporous graphene, Science 360 (6385) (2018) 199–203.
- [24] A. Sinitskii, A recipe for nanoporous graphene, Science 360 (6385) (2018) 154–155.
- [25] Y. Yang, X. Yang, L. Liang, Y. Gao, H. Cheng, X. Li, M. Zou, R. Ma, Q. Yuan, X. Duan, Large-area graphene-nanomesh/carbon-nanotube hybrid membranes for ionic and molecular nanofiltration, Science 364 (6445) (2019) 1057-1062.
- [26] J. Bai, X. Zhong, S. Jiang, Y. Huang, X. Duan, Graphene nanomesh, Nat. Nanotechnol. 5 (3) (2010) 190.
- [27] H. Lu, H. Wang, W. É, D. Dai, H. Fan, Z. Ma, X. Yang, On-surface fabrication of small-sized nanoporous graphene, J. Phys. Chem. C 123 (2019) 14404–14407.
- [28] Q. Zhou, Y. Ma, X. Ma, X. Luo, S. Zheng, Y. Nan, E. Ou, K. Wang, W. Xu, Synthesis of nanoporous graphenes via decarboxylation reaction, Chem. Commun. 56 (2020) 6336–6339.
- [29] G. Kresse, J. Hafner, Ab initiomolecular dynamics for liquid metals, Phys. Rev. B 47 (1993) 558.
- [30] G. Kresse, J. Hafner, Ab initiomolecular-dynamics simulation of the liquid-metal—amorphous-semiconductor transition in germanium, Phys. Rev. B 49 (1994) 14251.
- [31] S. Clark, M. Segall, C. Pickard, P. Hasnip, M. Probert, K. Refson, M. Payne, First principles methods using castep, Z. Kristallogr. 220 (2005) 567–570.
- [32] W. Tang, E. Sanville, G. Henkelman, A grid-based bader analysis algorithm without lattice bias, J. Phys. Condens. Matter 21 (2009), 084204.
- [33] G. Henkelman, H. Jónsson, A climbing image nudged elastic band method for finding saddle points and minimum energy paths, J. Chem. Phys. 113 (2000) 9901–9904.
- [34] G. Henkelman, H. Jónsson, Improved tangent estimate in the nudged elastic band method for finding minimum energy paths and saddle points, J. Chem. Phys. 113 (2000) 9978—9985.
- [35] J. Li, et al., Monolayer honeycomb borophene: a promising anode material with a record capacity for lithium-ion and sodium-ion batteries, J. Electrochem. Soc. 167 (9) (2020), 090527.
- [36] C. Yang, et al., Ultrahigh capacity of monolayer dumbbell C₄N as a promising anode material for lithium-ion battery, J. Electrochem. Soc. 167 (2020), 020538.
- [37] G. Kresse, D. Joubert, From ultrasoft pseudopotentials to the projector augmented-wave method, Phys. Rev. B 59 (1999) 1758.
- [38] P.E. Blochl, Projector augmented-wave method, Phys. Rev. B 50 (1994) 17953.
- [39] J. Moellmann, S. Grimme, DFT-D3 study of some molecular crystals, J. Phys. Chem. C 118 (14) (2014) 7615–7621.
- [40] J. Moellmann, S. Ehrlich, R. Tonner, S. Grimme, A DFT-D study of structural and energetic properties of Tio₂ modifications, J. Phys-Condens. Mat. 24 (42) (2012) 424206.
- [41] Z. Wang, S. Selbach, T. Grande, Van Der Waals, Density functional study of the energetics of alkali metal intercalation in graphite, RSC Adv. 4 (8) (2014)

- 4069-4079.
- [42] J. Wang, F. Li, X. Liu, H. Zhou, X. Shao, Y. Qu, M. Zhao, Cu₃N and its analogs: a new class of electrodes for lithium ion batteries, J. Mater. Chem. A 5 (18) (2017) 8762-8768.
- [43] J. Zhang, L. Xu, C. Yang, X. Zhang, L. Ma, M. Zhang, J. Lu, Two-dimensional single-layer PC₆ as promising anode materials for Li-ion batteries: the firstprinciples calculations study, Appl. Surf. Sci. (2020) 145493.
- [44] H. Huang, H. Wu, C. Chi, J. Zhu, B. Huang, T. Zhang, Out-of-Plane ion transport makes nitrogenated holey graphite a promising high-rate anode for both Li and Na ion batteries, Nanoscale 11 (40) (2019) 18758–18768.
- [45] L. Peng, P. Xiong, L. Ma, Y. Yuan, Y. Zhu, D. Chen, X. Luo, I. Lu, K. Amine, G. Yu. Holey two-dimensional transition metal oxide nanosheets for efficient energy storage, Nat. Commun. 15139 (8) (2017), 2041-1723.
- [46] S. Thinius, M. Islam, P. Heitjans, T. Bredow, Theoretical study of Li migration in lithium-graphite intercalation compounds with dispersion-corrected DFT methods, I. Phys. Chem. C 118 (5) (2014) 2273–2280.
- [47] C. Jiang, et al., Electrolyte-assisted dissolution-recrystallization mechanism towards high energy density and power density CF cathodes in potassium cell, Nano Energy 70 (2020) 104552.
- [48] J. Zheng, Z. Ren, P. Guo, L. Fang, J. Fan, Diffusion of Li+ ion on graphene: a DFT
- study, Appl. Surf. Sci. 258 (5) (2011) 1651–1655.
 [49] X. Zhang, et al., Monolayer GaS with high ion mobility and capacity as a promising anode battery, Material. J. Mater. Chem. A 7 (23) (2019) 14042-14050
- [50] J. Su, T. Duan, W. Li, B. Xiao, G. Zhou, Y. Pei, X. Wang, A first-principles study of 2D antimonene electrodes for Li ion storage, Appl. Surf. Sci. 462 (2018) 270 - 275
- [51] J. Liu, S. Wang, Q. Sun, All-carbon-based porous topological semimetal for Liion battery anode material, P. Natl. Acad. Sci. USA. 114 (4) (2017) 651–656.
- [52] J. Liu, S. Wang, Y. Qie, C. Zhang, Q. Sun, High-pressure-assisted design of porous topological semimetal carbon for Li-ion battery anode with high-rate performance, Phys. Rev. Mater. 2 (2) (2018), 025403.
- [53] C. Eames, M. Islam, Ion intercalation into two-dimensional transition-metal carbides: global screening for new high-capacity battery materials, J. Am. Chem. Soc. 136 (2014) 16270-16276.
- [54] M. Wang, Z. Yang, W. Li, L. Gu, Y. Yu, Preparation of nitrogen- and phosphorous Co-doped carbon microspheres and their superior performance as anode in sodium-ion batteries, Small 12 (2016) 2559–2566.
- [55] L. Fan, B. Lu, Reactive oxygen-doped 3D interdigital carbonaceous materials for Li and Na ion batteries, Small 12 (2016) 2783-2791.
- [56] H. Tsukada, K. Onda, H. Miyaji, S. Shiraishi, Y. Endo, Activated Carbon for Electrode of Power Storage Device and Method for Manufacturing Activated Carbon for Electrode of Power Storage Device, 2018. US10049824B2.
- [57] K. Azusa, K. Kei, N. Takeshi, F. Shun, S. Soshi, T. Hidehiko, K. Shinichi, Highcapacity hard carbon synthesized from macroporous phenolic resin for sodium-ion and potassium-ion battery, ACS Appl. Energy Mater. 3 (1) (2019) 135-140, 3.
- [58] X. Lin, Y. Liu, H. Tan, B. Zhang, Advanced lignin-derived hard carbon for Na-ion batteries and a comparison with Li and K ion storage, Carbon 157 (2020) 316-323.

[59] K. Wang, Y. Jin, S. Sun, Y. Huang, J. Peng, J. Luo, Q. Zhang, Y. Qiu, C. Fang, J. Han, Low-cost and high-performance hard carbon anode materials for sodium-ion batteries, ACS Omega 2 (4) (2017) 1687-1695.

- [60] H. Zhang, H. Ming, W. Zhang, G. Cao, Y. Yang, Coupled carbonization strategy toward advanced hard carbon for high-energy sodium-ion battery, ACS Appl. Mater. Interfaces 9 (28) (2017) 23766-23774.
- [61] A. Stevanus, C. Christian, K. Jaehoon, Extended plateau capacity of phosphorus-doped hard carbon used as an anode in Na- and K-ion batteries, Chem. Eng. J. 391 (2020) 123576.
- [62] H. Hou, C.E. Banks, M. Jing, Y. Zhang, X. Ji, Carbon quantum dots and their derivative 3D porous carbon frameworks for sodium-ion batteries with ultralong cycle life, Adv. Mater. 27 (2015) 7861-7866.
- [63] J. Xu, M. Wang, N. Wickramaratne, M. Jaroniec, S. Dou, L. Dai, High-performance sodium ion batteries based on a 3D anode from nitrogen-doped graphene foams, Adv. Mater. 27 (2015) 2042-2048.
- Y. Yan, Y. Yin, Y. Guo, L. Wan, A sandwich-like hierarchically porous carbon/ graphene composite as a high-performance anode material for sodium-ion batteries, Adv. Energy Mater. 4 (2014) 1301584.
- K. Smith, R. Parrish, W. Wei, Y. Liu, T. Li, Y. Hu, H. Xiong, Disordered 3D multilayer graphene anode material from CO2 for sodium-ion batteries, Chem-SusChem 9 (2016) 1397-1402.
- [66] K. Zhang, Q. He, F. Xiong, J. Zhou, Y. Zhao, L. Mai, L. Zhang, Active sites enriched hard carbon porous nanobelts for stable and high-capacity potassium-ion storage, Nano Energy 77 (2020) 105018.
- Z. Xing, Y. Qi, Z. Jian, X. Ji, Polynanocrystalline graphite: a new carbon anode with superior cycling performance for K-ion batteries, ACS Appl. Mater. Interfaces 9 (2017) 4343-4351.
- W. Yang, J. Zhou, S. Wang, Z. Wang, F. Lv, W. Zhang, W. Zhang, Q. Sun, S. Guo, A three-dimensional carbon framework constructed by N/S Co-doped graphene nanosheets with expanded interlayer spacing facilitates potassium ion storage, ACS Energy Lett. 5 (5) (2020) 1653–1661.
- [69] R. Cui, B. Xu, H. Dong, C. Yang, Q. Jiang, N/O dual-doped environment-friendly hard carbon as advanced anode for potassium-ion batteries, Adv. Sci. 7 (5) (2020) 1902547.
- [70] Y. Xu, C. Zhang, M. Zhou, Q. Fu, C. Zhao, M. Wu, Y. Lei, Highly nitrogen doped carbon nanofibers with superior rate capability and cyclability for potassium ion batteries, Nat. Commun. 9 (1) (2018), 1720-1720.
- [71] K. Narendra, S. Jorge, Lithium-ion model behavior in an ethylene carbonate electrolyte using molecular dynamics, J. Phys. Chem. C 120 (30) (2016) 16322-16332.
- [72] T. Li, P. Balbuena, Theoretical studies of lithium perchlorate in ethylene carbonate, propylene carbonate, and their mixtures, J. Electrochem. Soc. 146 (10) (1999) 3613-3622.
- [73] A. Karatrantos, S. Khan, T. Ohba, Q. Cai, The effect of different organic solvents on sodium ion storage in carbon nanopores, Phys. Chem. Chem. Phys. 20 (9) (2018) 6307-6315
- [74] H. Ota, Y. Sakata, A. Inoue, S. Yamaguchib, Analysis of vinylene carbonate derived sei layers on graphite anode, J. Electrochem. Soc. 151 (10) (2004) A1659-A1669.